Science of the Total Environment 621 (2018) 54–66

Contents lists available at ScienceDirect

Science of the Total Environment

journal homepage: www.elsevier.com/locate/scitotenv

Effects of soil type and rainfall intensity on sheet erosion processes and sediment characteristics along the climatic gradient in central-south China

Xinliang Wu [a], Yujie Wei [a], Junguang Wang [a,*], Jinwen Xia [a], Chongfa Cai [a,*], Zhiyuan Wei [a,b]

[a] Key Laboratory of Arable Land Conservation (Middle and Lower Reaches of Yangtze River) of the Ministry of Agriculture, College of Resources and Environment, Huazhong Agricultural University, Wuhan 430070, China
[b] Institute of Tropical Crops Genetic Resources, Chinese Academy of Tropical Agricultural Sciences, Danzhou, Hainan 571700, China

HIGHLIGHTS

- Soil type impact on sheet erosion was investigated by field plot experiments.
- Illite content was negatively correlated with average runoff coefficient ($p < 0.05$).
- Amorphous iron oxides and bulk density enhanced soil resistance to erosive forces.
- Sediment size generally increased from temperate Luvisol to tropical Ferralsol.
- This study facilitated a better understanding of the climate effect on soil erosion.

GRAPHICAL ABSTRACT

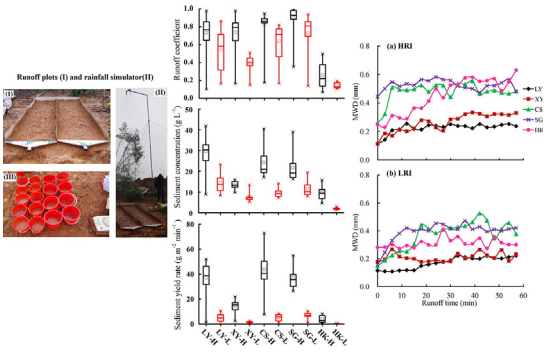

ARTICLE INFO

Article history:
Received 19 July 2017
Received in revised form 3 November 2017
Accepted 17 November 2017
Available online 22 November 2017

Editor: R Ludwig

Keywords:
Sheet erosion
Field plot
Erosion model
Sediment selectivity
Climate change

ABSTRACT

Soil erosion poses a major threat to the sustainability of natural ecosystems. The main objective of this study was to investigate the effects of soil type and rainfall intensity on sheet erosion processes (hydrological, erosional processes and sediment characteristics) from temperate to tropical climate. Field plot experiments were conducted under pre-wetted bare fallow condition for five soil types (two Luvisols, an Alisol, an Acrisol and a Ferralsol) with heavy textures (silty clay loam, silty clay and clay) derived separately from loess deposits, quaternary red clays and basalt in central-south China. Rainfall simulations were performed at two rainfall intensities (45 and 90 mm h^{-1}) and lasted one hour after runoff generation. Runoff coefficient, sediment concentration, sediment yield rate and sediment effective size distribution were determined at 3-min intervals. Runoff temporal variations were similar at the high rainfall intensity, but exhibited a remarkable difference at the low rainfall intensity among soil types except for tropical Ferralsol. Illite was positively correlated with runoff coefficient ($p < 0.05$). Rainfall intensity significantly contributed to the erosional process ($p < 0.001$). Sediment concentration and yield rate were the smallest for the tropical Ferralsol and sediment concentration was the largest for the temperate Luvisol. The regimes (transport and detachment) limiting erosion varied under the interaction of rainfall characteristics (intensity and duration) and soil types, with amorphous iron oxides and bulk density jointly enhancing soil resistance to erosive forces (Adj-$R^2 > 88\%$, $p < 0.001$). Sediment size was dominated by <0.1 mm size fraction for the Luvisols and bimodally distributed with the peaks at <0.1 mm and 1–0.5 mm size for the other soil

* Corresponding authors.
E-mail addresses: wuxinlianghzau@163.com (X. Wu), weyujay@gmail.com (Y. Wei), jgwang@mail.hzau.edu.cn (J. Wang), cfcai@mail.hzau.edu.cn (C. Cai).

https://doi.org/10.1016/j.scitotenv.2017.11.202

types. Exchangeable sodium decreased sediment size while rainfall intensity and clay content increased it (Adj-$R^2 = 96\%$, $p < 0.01$). These results allow to better understand the climate effect on erosion processes at the spatial-temporal scale from the perspective of soil properties.

1. Introduction

Soil erosion is the most widespread form of land degradation and has posed a major threat to the sustainability of natural ecosystems (Lal, 2001; Dlamini et al., 2011). Sediment losses are usually associated with organic matter, nutrients, heavy metals, pesticides and other contaminants, resulting in direct or indirect impact on on-site and off-site soil functions, aquatic, terrestrial and atmospheric ecosystems (Mchunu and Chaplot, 2012; Glendell and Brazier, 2014; Rickson, 2014). Soil erosion by water involves the processes of detachment, transport and deposition of soil particles or aggregates (Ellison, 1947). Understanding erosion processes and determining the controlling factors are necessary for erosion control and development of erosion prediction models.

Rainfall erosion generally results from the individual or combined action of raindrop impact and surface flow (Kinnell, 2005) and is influenced by many factors such as rainfall characteristics (rainfall intensity, duration and pattern), soil properties (soil texture, aggregate stability, bulk density, clay mineralogy and organic matter) and surface conditions (slope, vegetation cover, roughness, the type and extent of crust) (Martínez-Mena et al., 2002; Lado and Ben-Hur, 2004; Le Bissonnais et al., 2005; Malam Issa et al., 2006; Ran et al., 2012; Mahmoodabadi and Sajjadi, 2016; Wang et al., 2017). Among these factors, raindrop impact is an important erosive force, not only detaching soil materials but also enhancing sediment transport by overland flow (Zhang and Wang, 2017) while soil properties especially aggregate stability affect soil detachability and water infiltration (Le Bissonnais, 1996). The actual effects of rainfall intensity on erosion process vary with soil properties or soil type (Martínez-Mena et al., 2002; Asadi et al., 2007; Defersha and Melesse, 2012). For example, Martínez-Mena et al. (2002) reported that the predominant erosion processes in the calcareous colluvial soil and marl soil were dependent on and independent of rainfall intensity, respectively. Defersha and Melesse (2012) found that sediment concentration decreased with the increase of rainfall intensity for clay Vertisol, but it showed an opposite trend for the clay Cambisol and sandy clay loam Regosol. The interactions between soil properties and rainfall characteristics affect erosion processes through altering surface conditions such as crust that reduces water infiltration and soil detachability (Le Bissonnais et al., 2005; Carmi and Berliner, 2008; Mahmoodabadi and Sajjadi, 2016; Vaezi et al., 2017). As the crust matures, transition occurs from a transport capacity-limited system to a detachment-limited system in sediment delivery (Moore and Singer, 1990). The erosion processes generally vary in time and space due to the dynamic evolution of soil surface conditions during the rainfall event (Le Bissonnais et al., 2005; Kinnell, 2005; Wang et al., 2013).

Besides runoff and sediment yield, sediment size characteristics and temporal variation, especially the effective size of sediments, are necessary for a better quantification of sediment transport mechanism and rate (Asadi et al., 2007, 2011; Shi et al., 2012; Wang et al., 2014; Hancock et al., 2017). Kinnell (2005) summarized six sediment transport models: raindrop splash, raindrop-induced saltation, raindrop-induced rolling, flow-driven saltation, flow-driven rolling and suspension, all of which depend on sediment properties (size, density and shape) and flow hydraulic characteristics (depth, velocity and turbulence) (Kinnell, 2006, 2012; Asadi et al., 2011; Shi et al., 2012). Coarse material is transported as rolling or saltation while the fine material remains suspended (Kinnell, 2006). As flow velocity increases, the dominant transport modes change from raindrop-induced rolling/saltation to flow-driven rolling/saltation (Kinnell, 2005; Asadi et al., 2007). Asadi et al. (2007, 2011) reported that the bimodal distribution of sediment size resulted from the two transport mechanisms of rolling and suspension/saltation in the coarser and finer size classes, respectively. The sediment properties are usually inherited from original soils and thus vary with soil types (Martínez-Mena et al., 2002; Malam Issa et al., 2006; Asadi et al., 2007; Wang et al., 2014). Compared to sediment amount, less research attention has been paid to the sediment size distribution, let alone at the field scale.

To date, most studies are focused on the climate effect on soil erosion mainly in terms of precipitation, vegetation and land use (Cerdà, 1998; Nearing et al., 2004; Ruiz-Sinoga and Diaz, 2010; Serpa et al., 2015) and few efforts have been made to investigate erosion processes response to climate change from the perspective of soil properties or types (Salvador Sanchis et al., 2008). As an indicator of soil resistance to erosion, aggregate stability has been verified to be influenced by soil type or climate condition (Six et al., 2002; Wu et al., 2016). Soil erodibility widely used in empirical models (USLE or RUSLE) for various soil types is generally applicable to predict the long-term average soil loss and that in the process-based models (WEPP) is mainly based on soil texture, both of which do not take into account the temporal variations during the rainfall events (Kinnell, 2005, 2017; Wang et al., 2013). In addition, despite intensive experiments performed on the erosion of various types of soils, these data cannot explain the general mechanism underlying erosion processes due to the incomparability of experimental conditions (Malam Issa et al., 2006; Knapen et al., 2007; Gumiere et al., 2009; Kinnell, 2016). Therefore, a systematic investigation with field experiments, although costly and laborious, is necessary for a better understanding of the specific erosion processes of different types of soils.

The main objective of this study was to investigate the effects of soil type and rainfall intensity on sheet erosion processes (hydrological, erosional response and sediment size characteristics) along the climate gradient. It is hypothesized that the susceptibility of surface soils to rainfall erosion varies with the physicochemical nature of soils which mainly results from climate conditions and that there exists a significant difference in sediment sizes and transport mechanisms among different soil types. In this study, field plot rainfall simulation experiments were conducted on bare fallow soils with an increased weathering gradient from temperate to topical climate. When isolating the effects of soil type and rainfall intensity on sheet erosion, the factors such as plot size, land use, slope gradient, soil texture, profile constitution and soil surface conditions were maintained as uniform as possible.

2. Materials and methods

2.1. Experimental sites and soils

Based on the principle of typicality of soil types and accessibility of field rainfall simulation, five typical soils were selected and the experimental sites were separately located in Luoyang city (LY) in Henan province, Xiangyang city (XY) in Hubei province, Changsha city (CS) in Hunan province, Shaoguan city (SG) in Guangdong province, and Haikou city (HK) in Hainan province from north to south in central-south China (Fig. 1-a). The experimental sites fall separately into the warm temperate, northern subtropical, mid-subtropical, southern subtropical and tropical region and in East Asian Monsoon climate with the mean annual precipitation ranging from 650 to 1778 mm and the mean annual temperature from 13.7 to 24.2 °C. In this study region, water erosion

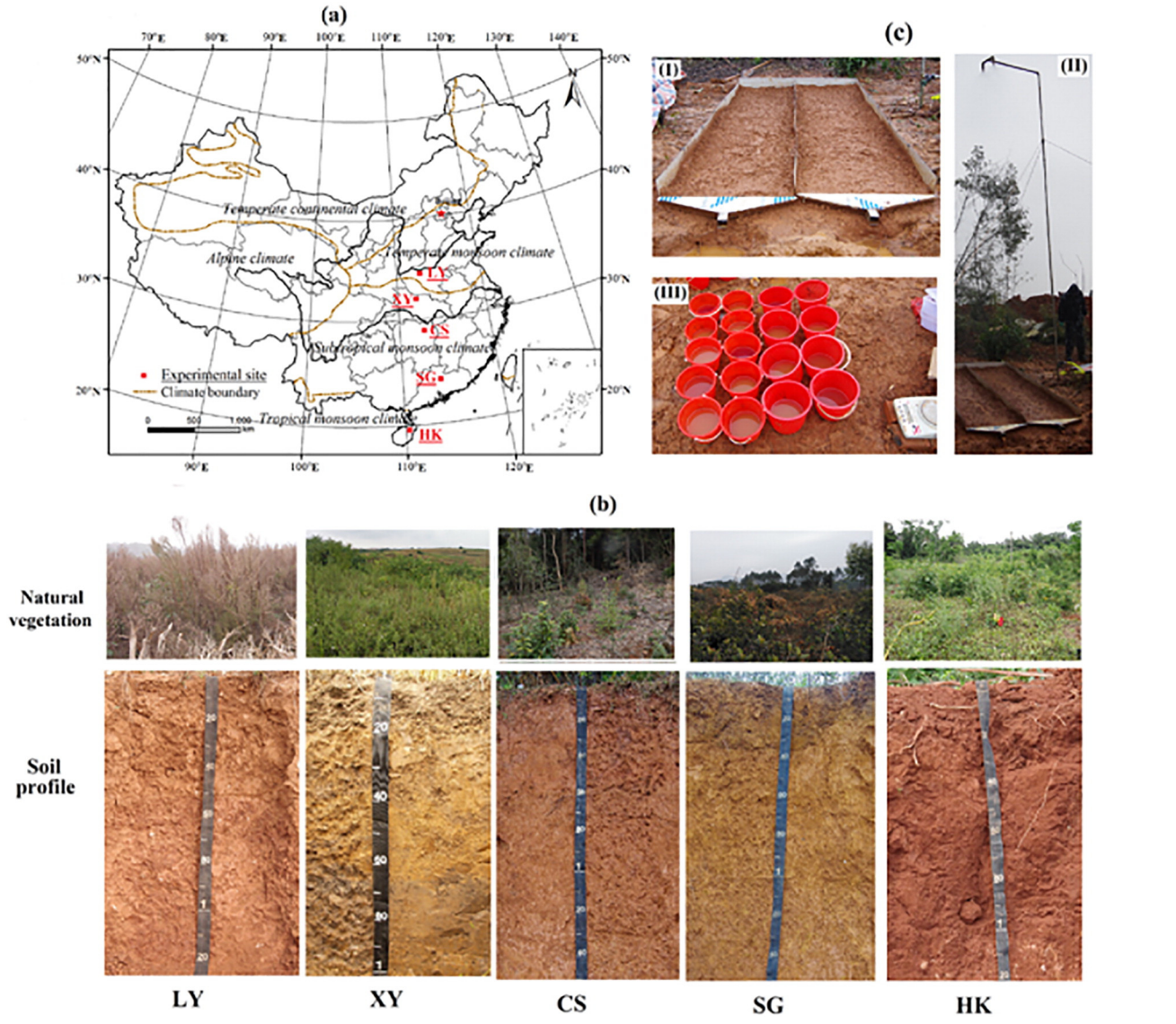

Fig. 1. Distribution of experimental sites (a), natural vegetations and soil profiles (b) and field experiment components (c) including (I) field plot, (II) rainfall simulator and (III) sample buckets. LY, Calcic Luvisol; XY, Ferric Luvisol; CS, Plinthic Alisol; SG, Plinthic Acrisol; HK, Acric Ferralsol.

has been a threat to land productivity and environment quality due to long-term poor land use and management. The hilly land constitutes the main farmland resource, with sheet, rill and interrill erosion commonly occurring on cultivated land.

The selected soils were classified into Calcic Luvisol (LY), Ferric Luvisol (XY), Plinthic Alisol (CS), Plinthic Acrisol (SG) and Acric Ferralsol (HK) (IUSS Working Group WRB, 2014). Correspondingly, soil weathering degree increased with an increase of hydrothermal conditions (Wu et al., 2016). The experimental soils were selected from soils with a similar heavy texture (silty clay loam, silty clay and clay) and a thick regolith that derived from loess deposit, quaternary red clay and basalt, respectively (Table 1). For each soil type, the experiment plots were prepared separately on soils with intact pedogenic horizons consisting of eluvial, illuvial and parent material horizons (Fig. 1-b). To avoid the anthropogenic impact on soil structure to different extents, land uses were chosen as natural vegetation cover such as grassland or forest land without tillage practice on the top soils. All the surface soils were in granular structure. The basic information of experimental sites and soils is summarized in Table 1.

Before field rainfall simulation, composited soil samples were collected from the top 10 cm soil layer in the areas within the prepared site adjacent to plots. Undisturbed soil cores (100 cm^3) were taken for

Table 1
Basic information of experimental sites and soils.

Code	Latitude/N	Longitude/E	Elevation (m)	MAP (mm)	MAT (°C)	Topography	Soil color (dry)	§Soil texture	Parent material
LY	34°48′14″	112°21′28″	335	650	13.7	Loess hill	7.5YR 5/4	Silty clay loam	Loess deposit
XY	32°07′50″	112°16′25″	104	878	16.0	Rolling hill	7.5YR 5/4	Silty clay	Loess deposit
CS	28°29′33″	112°54′13″	73	1422	17.1	Hilly land	7.5YR 6/6	Silty clay	Quaternary red clay
SG	24°19′06″	113°58′42″	128	1778	20.4	Piedmont terrace	7.5YR 6/6	Clay	Quaternary red clay
HK	19°52′26″	110°33′57″	22	1722	24.2	Platform	2.5YR 4/4	Clay	Basalt

Note: LY, Calcic Luvisol; XY, Ferric Luvisol; CS, Plinthic Alisol; SG, Plinthic Acrisol; HK, Acric Ferralsol; MAP, mean annual precipitation; MAT, mean annual temperature. §, soil texture classes are defined according to USDA recommendations.

the analysis of bulk density in quadruplicate. The field-moist soil samples were collected and gently broken up manually to enable the large clods to break along natural fissures. After removing large roots and other fresh organic materials, the samples were then fully air-dried and ground through different size sieves for physical and chemical analysis.

2.2. Soil property measurement

Basic soil properties were determined by standard analytical methods (Zhang and Gong, 2012). Specifically, bulk density (BD) were determined on undisturbed soil core (100 cm^3) by the weight method; pH by the potentiometric method at 1:2.5 soil/water mass ratio; soil organic carbon (SOC) by acid potassium-dichromate digestion; exchange base cations (Ca^{2+}, Mg^{2+}, K^+ and Na^+) by ammonium acetate exchange method; particle density (G_s) by pycnometry; soil texture by wet sieving-pipette method after dispersion; clay mineral types and their relative content in clay fraction by X-ray diffraction (XRD) after pre-treatment (Li, 1997). The content of every clay mineral type (mainly vermiculite, illite, 1.4 nm intergrade mineral and kaolinite) in soil was obtained by multiplying clay content (%) and the relative content (%) of clay mineral in clay fraction. The fractions of free iron (Fe_d) and aluminum (Al_d) oxides, and those of amorphous iron (Fe_o) and aluminum (Al_o) oxides were extracted using citrate- bicarbonate-dithionite (CBD) and ammonium oxalate, respectively (Zhang and Gong, 2012). Fe and Al concentrations in the extracts were determined by Inductively Coupled Plasma Optical Emissions Spectrometry (ICP-OES) (VISTA-MPX, Varian, America) after dilution.

Aggregate stability was measured by the routine dry- and wet-sieving methods (Kemper and Rosenau, 1986). Aggregate size distribution was characterized by the mean weight diameter (MWD). MWD_{dry} and MWD_{wet} denote the MWD of soil aggregates in the dry and wet sieving methods, respectively. Detailed procedures and calculations have been reported in a previous paper (Wu et al., 2016). All measurements were run in triplicate and averaged for statistical analysis.

Mean weight diameter (MWD) of soil aggregates and sediments was calculated using the following formula:

$$\mathrm{MWD} = \sum_{1}^{n+1} \frac{r_{i-1} + r_i}{2} \times m_i \quad (1)$$

where r_i, aperture of the ith mesh (mm), $r_0 = r_1$, $r_n = r_{n+1}$; m_i, mass percentage of aggregates remaining on ith sieve; n, number of the sieves.

2.3. Field plot rainfall simulation

Field rainfall simulation experiments were conducted from July 2015 to May 2016. Experimental erosion plots of 2.40 m^2 (length 3.00 m × width 0.80 m, at a slope of 10°, a representative slope gradient in hilly region) were used to investigate the sheet erosion. The plots were oriented parallel to the length of the hillslope (Fig. 1-c). Aluminum-plastic composite plates (length 3.00 m × width 0.25 m) were inserted into the soil to a depth of 0.15 m as plot boundaries with plant residues and root biomass removed from the plot. The flat and bare fallow surface was prepared by crushing the big clods (<3 cm) in the top 5 cm of the soils to simulate the cropland condition with a spade and rake. In order to keep the consistency in antecedent soil water condition, the plots were fully rewetted under the rainfall intensity of 45 mm h^{-1} with a 2-mm wire screen suspended 0.10 m above the soil surface to retard raindrop energy, until the runoff appeared at the outlet of plot and then the plots stood for 12 h to drain the free water before rainfall experiment. The antecedent soil water content varied in 0.31–0.44 cm^3 cm^{-3}. The plots at each rainfall intensity (45 and 90 mm h^{-1}) were set in duplicate (Fig. 1-c) and four plots were installed at each location.

Rainfall was simulated with a portable rainfall simulator (Luk et al., 1986) consisting of a SPRACO cone jet nozzle with a height of 5.0 m above the center of the plots and thus rain drops reached the soil surface with energy close to that of natural raindrops. The median drop size was 2.4 mm with a uniformity of 90% under the water pressure of 0.08 MPa (Cai et al., 2005). Rainfall intensity in the erosion test was designed as 45 mm h^{-1} (low) and 90 mm h^{-1} (high) with one and two nozzles, respectively. The rainstorms of two intensities were representative and common in the study region. To avoid wind influence, rainfall simulation was carried out in the windless days or under the protection of wind shield (6 m height and 4 m width) in the prevailing wind direction. Actual rainfall intensity and uniformity were monitored using eight cups placed at the border of the plot. The actual rainfall intensities were respectively 46 ± 4 and 104 ± 8 mm h^{-1} with a uniformity of 85–92% in the field condition.

The rainfall duration was 1 h after the initiation of runoff. Following the initiation of runoff, runoff and sediment were collected at 3-min intervals in plastic containers and the duration for sampling every time was dependent on the runoff rate with 2 min at the early stage of runoff and 1 min at the late stage. After weighing the total mass, the collected runoff and sediments were transferred to the plastic bottles and then taken back to the laboratory. During the rainfall process, no rills were observed for all the experimental plots.

2.4. Runoff and sediment measurement

The effective sediment size distribution was determined according to the method of aggregate fractionation proposed by Le Bissonnais (1996). Specifically, the water-sediment mixture sample in every plastic bottle was transferred on the 0.1 mm sieve and then immersed in water entirely and moved up and down 20 times to separate the fraction <0.1 mm from those >0.1 mm. The <0.1 mm faction in water was flocculated by adding 0.5 M $CaCl_2$ solution. After clear separation, the supernatant was sucked out and the faction settled on the bottom was transferred, oven-dried at 50 °C and weighed. The >0.1 mm fraction was collected in the beaker, oven-dried (50 °C) and gently dry-sieved by hand on a nest of five sieves (5, 2, 1, 0.5 and 0. 25 mm). The mass of each size fraction was weighed. Total sediment mass was the sum of the six fractions (5–2, 2–1, 1–0.5, 0.5–0.25, 0.25–0.1 and <0.1 mm) (Ignoring the mass of the flocculating agent due to its small amount). To better understand the sediment transport mechanisms, the effective size distribution rather than the dispersed particle sizes of sediments was analyzed in this study. Mean weight diameter (MWD) was used to characterize the sediment effective size composition according to Eq. (1).

The runoff volume is the difference between total sample mass and sediment mass (assuming the water density as 1 g mL^{-1}). Runoff coefficient was determined as the ratio of runoff rate (mm min^{-1}) to rainfall intensity (mm min^{-1}). Sediment concentration (g L^{-1}) was calculated as the sediment mass divided by the runoff volume. Sediment yield rate (g m^{-2} min^{-1}) was determined as the ratio of sediment yield (g) to sampling duration (min) and plot area (m^2).

2.5. Data analysis

The effects of soil type and rainfall intensity on erosion process indices (such as runoff coefficient, sediment concentration, sediment yield rate and sediment size) were tested by the ANOVA method ($p < 0.05$). Correlation analysis was made for variables at the significant level of 0.05, 0.01 and 0.001. Multiple stepwise linear regression was used to quantify the effects of soil properties and rainfall intensity on sheet erosion characteristics (including the average runoff coefficient, sediment concentration, sediment yield rate and sediment size). Due to the large magnitude variation, the sediment yield rate (S_Y) between rainfall

Table 2
Physicochemical properties of experimental soils (mean ± standard deviation, n = 3).

Code	LY	XY	CS	SG	HK
G_s	2.65 ± 0.01	2.65 ± 0.00	2.70 ± 0.00	2.80 ± 0.01	2.84 ± 0.01
pH	7.7 ± 0.05	6.5 ± 0.02	4.0 ± 0.02	4.7 ± 0.12	4.9 ± 0.01
SOC (%)	1.69 ± 0.15	0.46 ± 0.01	2.59 ± 0.01	0.96 ± 0.01	1.60 ± 0.01
$exCa^{2+}$ (cmol kg^{-1})	16.4 ± 0.2	7.8 ± 0.1	0.1 ± 0.0	0.2 ± 0.0	1.1 ± 0.1
$exMg^{2+}$ (cmol kg^{-1})	1.5 ± 0.1	2.7 ± 0.0	0.1 ± 0.0	0 ± 0	0.6 ± 0
$exNa^{+}$ (cmol kg^{-1})	0.3 ± 0.1	0.3 ± 0.0	0.1 ± 0.0	0.1 ± 0.1	0.2 ± 0.0
exK^{+} (cmol kg^{-1})	0.4 ± 0.0	0.4 ± 0.0	0.2 ± 0.0	0.1 ± 0.0	0.1 ± 0.0
BD (g cm^{-3})	1.22 ± 0.04	1.40 ± 0.08	1.13 ± 0.06	1.25 ± 0.07	1.13 ± 0.08
Fe_d (g kg^{-1})	15.4 ± 0.5	21.8 ± 0.2	40.9 ± 0.7	111.2 ± 0.5	145.1 ± 0.1
Al_d (g kg^{-1})	2.3 ± 0.1	4.5 ± 0.1	12.2 ± 0.2	34.0 ± 0.7	28.6 ± 0.1
Fe_o (g kg^{-1})	2.0 ± 0.1	2.4 ± 0.1	4.0 ± 0.0	3.1 ± 0.2	7.2 ± 0.2
Al_o (g kg^{-1})	2.1 ± 0.1	2.7 ± 0.0	5.2 ± 0.2	3.2 ± 0.1	4.5 ± 0.1
Sand (%)	7 ± 1	4 ± 0	7 ± 1	14 ± 0	18 ± 2
Silt (%)	63 ± 1	50 ± 3	42 ± 1	17 ± 2	16 ± 3
Clay (%)	30 ± 0	46 ± 3	51 ± 0	69 ± 2	66 ± 2
MWD_{dry} (mm)	2.72 ± 0.28	3.60 ± 0.12	3.25 ± 0.21	2.85 ± 0.19	2.04 ± 0.05
MWD_{wet} (mm)	0.35 ± 0.03	1.28 ± 0.05	1.39 ± 0.06	1.34 ± 0.05	1.78 ± 0.09

Note: LY, Calcic Luvisol; XY, Ferric Luvisol; CS, Plinthic Alisol; SG, Plinthic Acrisol; HK, Acric Ferralsol; G_s, particle density; SOC, soil organic carbon; BD, bulk density (n = 4); $exCa^{2+}$, $exMg^{2+}$, $exNa^{+}$ and exK^{+}, exchangeable calcium, magnesium, sodium and potassium ions; Fe_d and Al_d, free iron and aluminum oxides; Fe_o and Al_o, amorphous iron and aluminum oxides; Sand, 2–0.05 mm; Silt, 0.05–0.002 mm; Clay, <0.002 mm; MWD_{dry} and MWD_{wet} indicate the mean weight diameters of air-dried and water stable aggregates, respectively.

intensities was treated with logarithmic transformation ($\ln(S_V)$) before stepwise regression analysis. All data analysis was performed using the SPSS16.0 software (Xue, 2013).

3. Results

3.1. Physicochemical properties

Basic physicochemical properties of selected soils are summarized in Table 2. Soil pH was around neutral for LY and XY and shifted to strongly acidic for CS, SG and HK. Correspondingly, the exchange base cation content decreased, particularly for the calcium and magnesium ions. Soil particle density, free oxides and clay content (30%–69%) generally increased from LY to HK while silt content (16%–63%) followed an inverse pattern. The soils were classified as silty clay loam (LY), silty clay (XY and CS) and clay (SG and HK), respectively. Compared to free oxides, amorphous oxides content was much lower (2.0–7.2 g kg^{-1} for Fe_o and 2.1–5.2 g kg^{-1} for Al_o). Soil organic carbon (0.46–2.59%) and bulk density (1.13–1.40 g cm^{-3}) did not show a distinct trend from LY to HK.

As shown in Fig. 2, the clay fraction was dominated by vermiculite, illite and kaolinite for LY and XY, kaolinite and illite for CS and SG and kaolinite for HK with a small amount of 1.4 nm intergrade minerals. The relative content of kaolinite generally increased and that of illite decreased from LY to HK.

Mean weight diameters of air-dried aggregates (MWD_{dry}) and water stable aggregates (MWD_{wet}) ranged from 2.04–3.60 mm and 0.35–1.78 mm, respectively (Table 2). MWD_{dry} decreased from XY to HK. The largest and smallest of MWD_{wet} appeared in LY and HK, respectively and no significant differences in MWD_{wet} occurred among XY, CS and SG. Spearman correlations indicated that MWD_{dry} was negatively correlated with sand content ($r = -0.90$, $p < 0.05$) and MWD_{dry} was positively correlated with amorphous iron oxides ($r = 0.98$, $p < 0.01$).

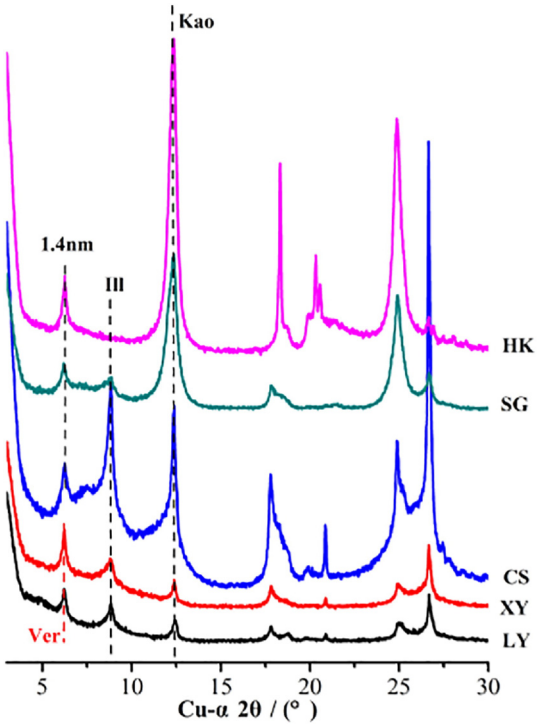

Fig. 2. Clay mineralogy of different soil types. Kao, kaolinite; Ill, illite; 1.4 nm, 1.4 nm intergrade minerals; Ver, vermiculite. LY, Calcic Luvisol; XY, Ferric Luvisol; CS, Plinthic Alisol; SG, Plinthic Acrisol; HK, Acric Ferralsol.

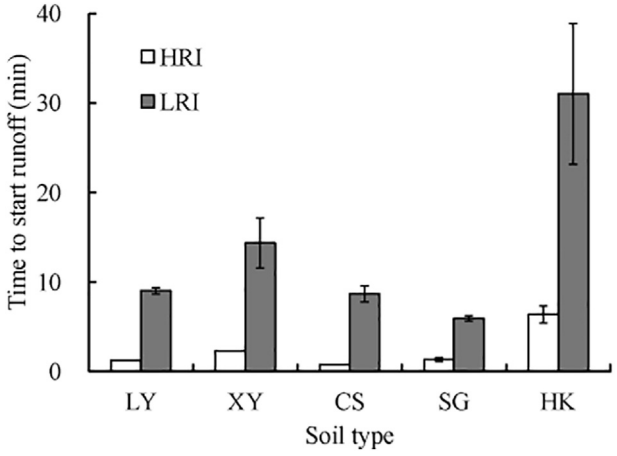

Fig. 3. Time to start runoff (T_r) for different soil types and rainfall intensities. HRI, high rainfall intensity (90 mm h^{-1}); LRI, low rainfall intensity (45 mm h^{-1}). LY, Calcic Luvisol; XY, Ferric Luvisol; CS, Plinthic Alisol; SG, Plinthic Acrisol; HK, Acric Ferralsol. The error bar indicates the standard deviation of two replicates.

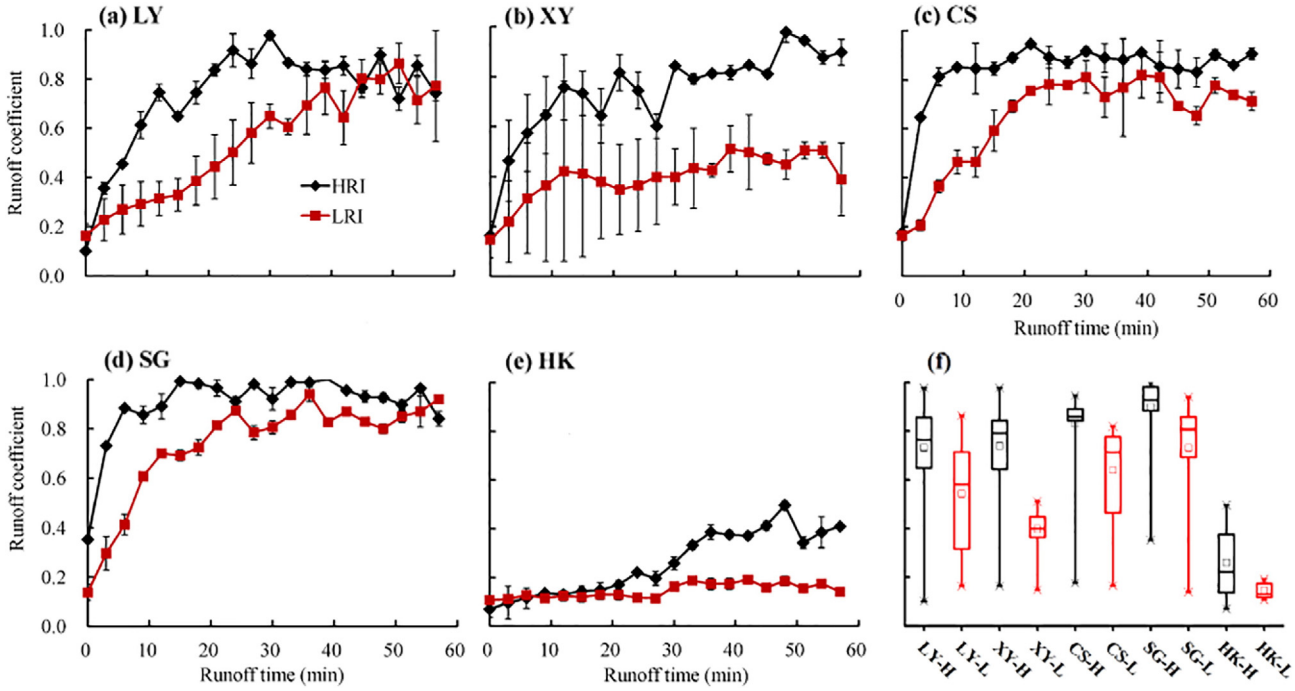

Fig. 4. Temporal variations in runoff coefficient for different soil types and rainfall intensities. LY, Calcic Luvisol; XY, Ferric Luvisol; CS, Plinthic Alisol; SG, Plinthic Acrisol; HK, Acric Ferralsol; HRI, high rainfall intensity (90 mm h^{-1}); LRI, low rainfall intensity (45 mm h^{-1}). In subfigure (f), "-H" and "-L" indicate the high (90 mm h^{-1}) and low (45 mm h^{-1}) rainfall intensities, respectively; the boxes indicate the 25th and 75th percentiles; the line in the box indicates the median (50th percentile); "×" indicates max-min values; "□" indicates the average value. The error bar indicates the standard deviation of two replicates.

3.2. Hydrological response

The time to start runoff (T_r) was more than four times longer at the low than at the high rainfall intensity (Fig. 3). For example, T_r for CS was 0.78 min and 8.68 min at the high and low rainfall intensities, respectively. It indicated that rainfall intensity greatly influenced surface soil infiltration at the early stage of rainfall. T_r of HK was the largest (6.38 and 31.03 min for the high and low rainfall intensities, respectively) in all the soil types regardless of rainfall intensity.

Runoff coefficient generally increased at the early stage and then approached a quasi-steady state (Fig. 4). High rainfall intensity contributed to the shift from increase trend to quasi-steady state. The effects of

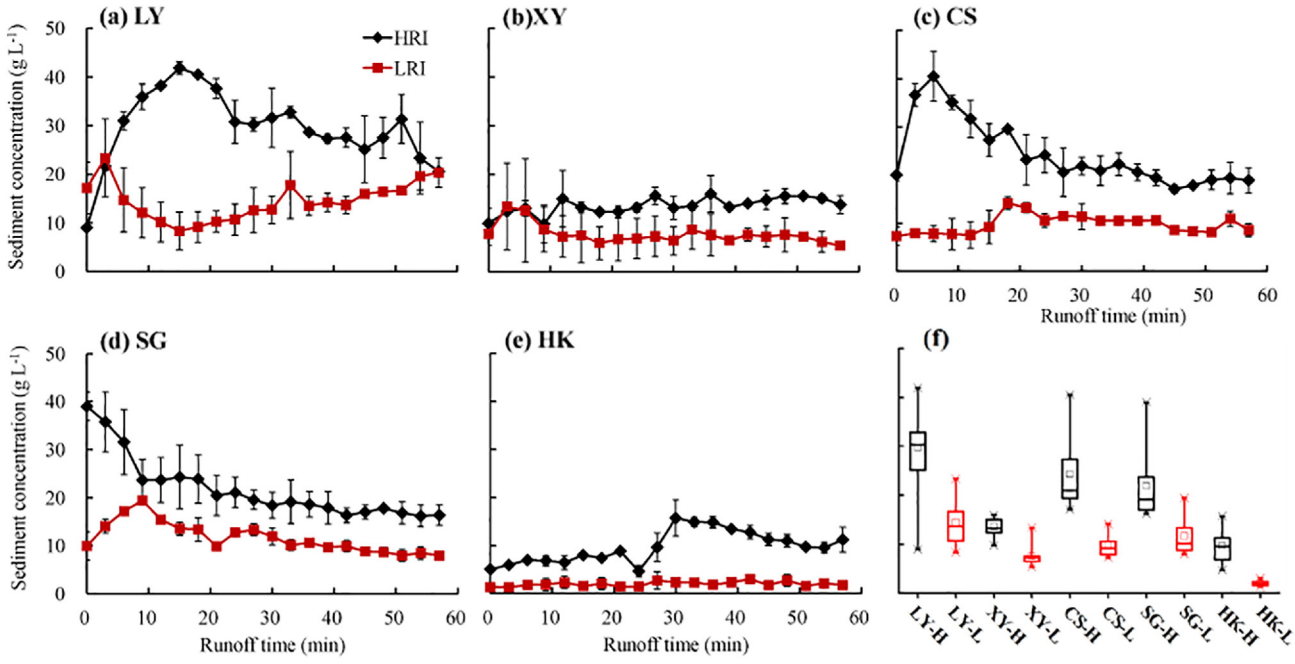

Fig. 5. Temporal variations in sediment concentration for different soil types and rainfall intensities. LY, Calcic Luvisol; XY, Ferric Luvisol; CS, Plinthic Alisol; SG, Plinthic Acrisol; HK, Acric Ferralsol; HRI, high rainfall intensity (90 mm h^{-1}); LRI, low rainfall intensity (45 mm h^{-1}). In subfigure (f), "-H" and "-L" indicate the high (90 mm h^{-1}) and low (45 mm h^{-1}) rainfall intensities, respectively; the boxes indicate the 25th and 75th percentiles; the line in the box indicates the median (50th percentile); "×" indicates max-min values; "□" indicates the average value. The error bar indicates the standard deviation of two replicates.

rainfall intensity on runoff generation differed between soil types. For soils LY, CS and SG, R_c was significantly larger at the high than at the low rainfall intensity at the initial stage and then their difference in R_c decreased to zero or non-significant. In contrast, for XY and HK, at the early stage of runoff, the difference in R_c was non-significant and then increased to a relative steady value as rainfall continued. The average R_c was generally larger at the high than the low rainfall intensity. Among these soil types, R_c was lowest (<0.50) for HK regardless of rainfall intensity. For the other soil types, the dynamic of R_c was similar at the high rainfall intensity, but it showed a remarkable difference between soil types at the low rainfall intensity (Fig. 4-f).

3.3. Erosional response

The temporal variations in sediment concentration (C_s) for different soil types and rainfall intensities are presented in Fig. 5. For LY, CS and HK, the C_s at the high rainfall intensity peaked early during the runoff event before the subsequent decrease towards a steady state, while the temporal variation of C_s was more subdued at the low rainfall intensity. For SG at the high rainfall intensity, the C_s decreased rapidly after runoff initiation and then slightly leveled off during the rainfall event. The magnitude of C_s variation was relatively smaller at the low than at the high rainfall intensity (Fig. 5-f), and the sediment concentration was obviously larger at the high than at the low rainfall intensity ($p < 0.05$). For HK, the average C_s (9.7 g L^{-1}) at the high rainfall intensity was more than four times (4.9) larger than that (1.9 g L^{-1}) at the low rainfall intensity. There was significant difference between different soil types. Similar to runoff generation, the C_s was lowest (<15.7 g L^{-1}) for HK regardless of rainfall intensity, followed by soil XY (<16.0 g L^{-1}), and highest C_s for LY (<41.9 g L^{-1}).

Sediment yield rate (S_Y) varied obviously with soil types and rainfall intensities (Fig. 6). It increased at the early stage of runoff, followed by its temporal variations in several patterns: (i) a slight decline after reaching the peak, such as SG, LY and CS at the high rainfall intensity; (ii) reaching a quasi-steady state such as HK, and CS at the low rainfall intensity; (iii) a slight increase, such as LY at the low rainfall intensity and XY at the high rainfall intensity. Sediment yield rate was overall significantly larger at the high than at the low rainfall intensity ($p < 0.05$) and the average sediment yield rate at the high rainfall intensity (4.1–43.7 g m^{-2} min^{-1}) was 5.2 (SG) ~17.4 (HK) times that at the low rainfall intensity (0.2–7.2 g m^{-2} min^{-1}). The positive effect of rainfall intensity on the sediment yield rate was dependent on the soil type and rainfall duration. For LY, CS and SG, the difference in the sediment yield rate between rainfall intensities increased at the early stage of runoff, followed by a decrease as rainfall continued and for XY and HK, the difference increased gradually and then reached to a steady state. Among all soil types (Fig. 6-f), the average sediment yield rate was lowest for HK, followed by XY, and both of them was much lower than LY, CS and SG which showed no significant difference in the sediment yield rate due to slight variations in their rainfall intensities (46 ± 4 and 104 ± 8 mm h^{-1}). These data indicated that sediment yield was influenced by the interaction of soil types and rainfall characteristics (intensity and duration), with no distinct trend observed along the climate gradient.

3.4. Sediment size characteristics

At the early stage of runoff, the percentage of <0.1 mm size sediments declined while that of the coarser size sediments (such as 1–0.5 mm size) increased (Fig. 7). As rainfall continued, the contents of all these size sediments reached a quasi-steady state. High rainfall intensity contributed to the output of coarse size sediments (>0.25 mm), especially for CS, SG and HK. For LY and XY, the sediment was principally composed of <0.1 mm size fraction occupying >70% of the total sediment mass. For CS and SG, the sediments were still dominated by the <0.1 mm size fraction (>50%) at the early stage of high rainfall intensity

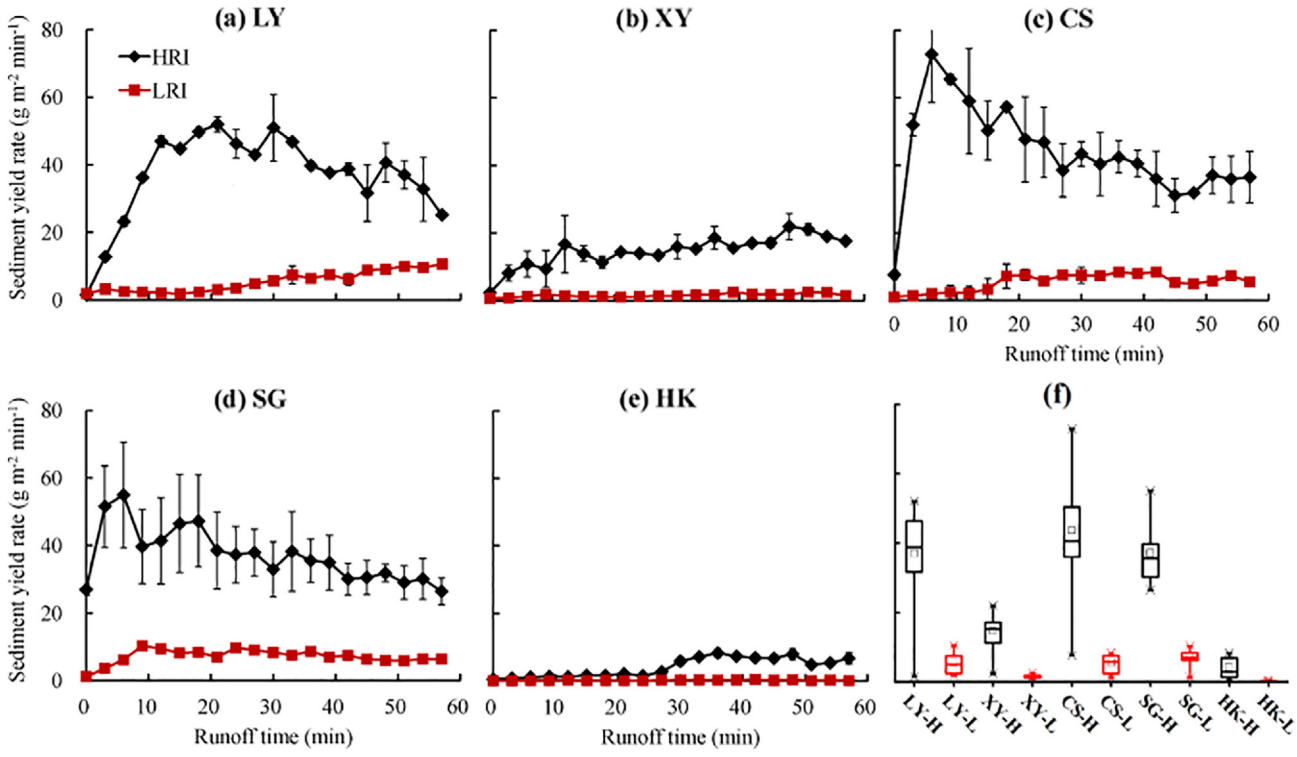

Fig. 6. Temporal variations in sediment yield rate for different soil types and rainfall intensities. LY, Calcic Luvisol; XY, Ferric Luvisol; CS, Plinthic Alisol; SG, Plinthic Acrisol; HK, Acric Ferralsol; HRI, high rainfall intensity (90 mm h^{-1}); LRI, low rainfall intensity (45 mm h^{-1}). In subfigure (f), "-H" and "-L" indicate the high (90 mm h^{-1}) and low (45 mm h^{-1}) rainfall intensities, respectively; the boxes indicate the 25th and 75th percentiles; the line in the box indicates the median (50th percentile); "×" indicates max-min values; "□" indicates the average value. The error bar indicates the standard deviation of two replicates.

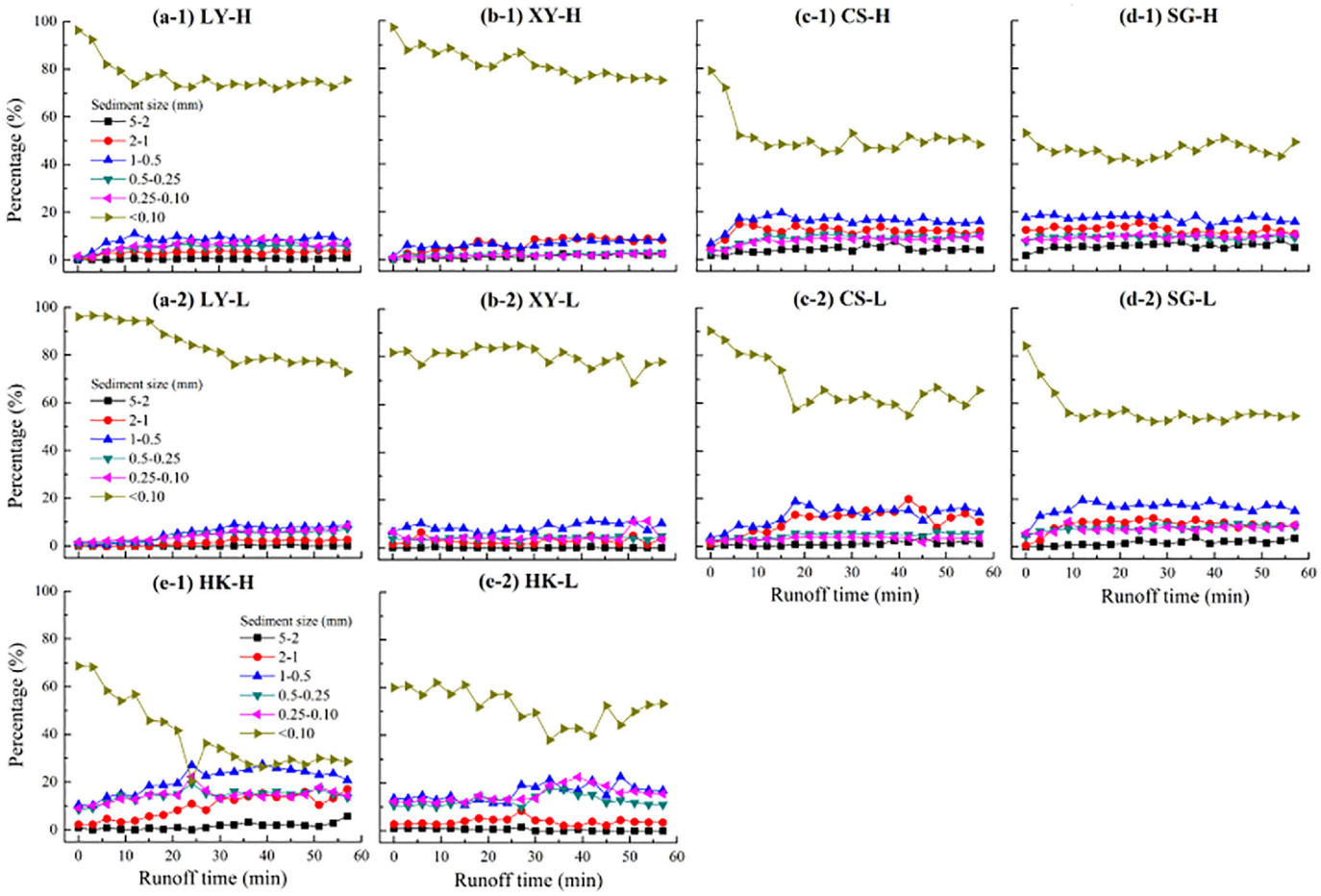

Fig. 7. Temporal variations in sediment size for different soil types and rainfall intensities (n = 2). LY, Calcic Luvisol; XY, Ferric Luvisol; CS, Plinthic Alisol; SG, Plinthic Acrisol; HK, Acric Ferralsol; "-H" and "-L" indicate the high (90 mm h^{-1}) and low (45 mm h^{-1}) rainfall intensities, respectively.

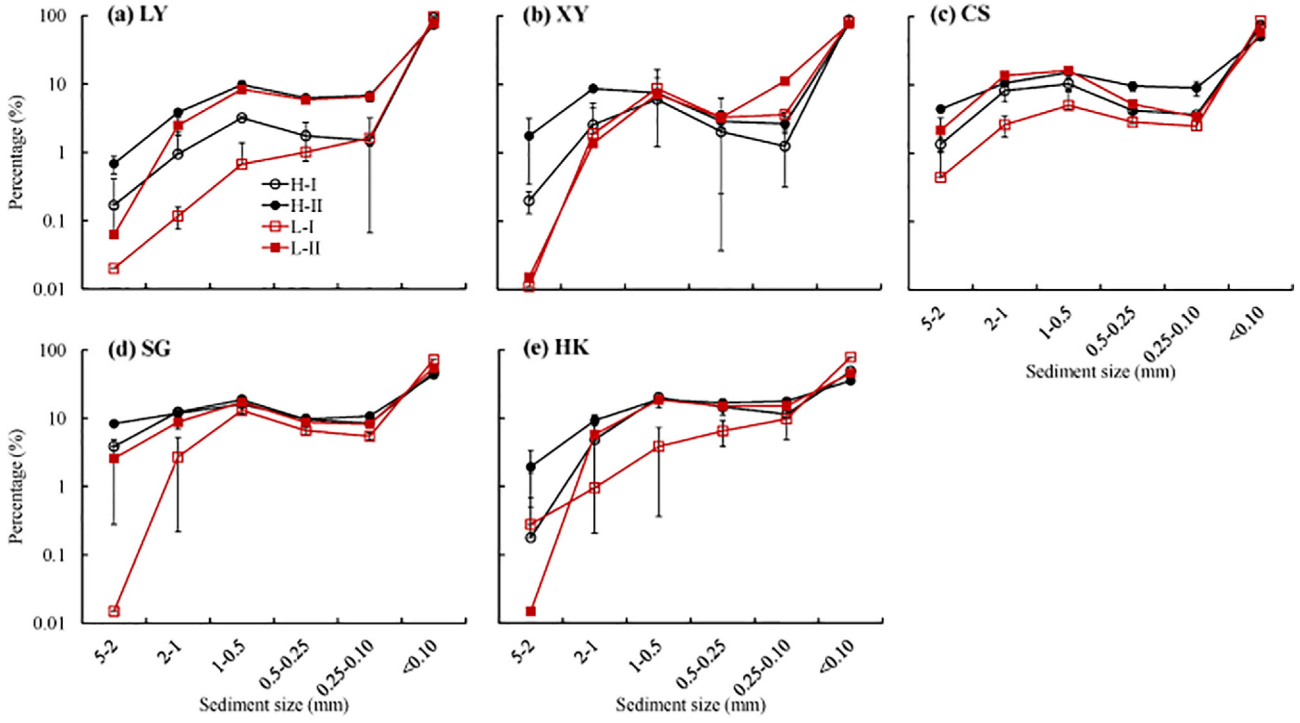

Fig. 8. Effective sediment size distributions at two sampling times for different soil types and rainfall intensities. LY, Calcic Luvisol; XY, Ferric Luvisol; CS, Plinthic Alisol; SG, Plinthic Acrisol; HK, Acric Ferralsol; "H-I" and "H-II" indicate the sampling times of 3–6 min and 54–57 min at the high (90 mm h^{-1}) rainfall intensity, respectively; "L-I" and "L-II" indicate the sampling times of 3–6 min and 54–57 min at the low (45 mm h^{-1}) rainfall intensity, respectively. The error bar indicates the standard deviation of two replicates.

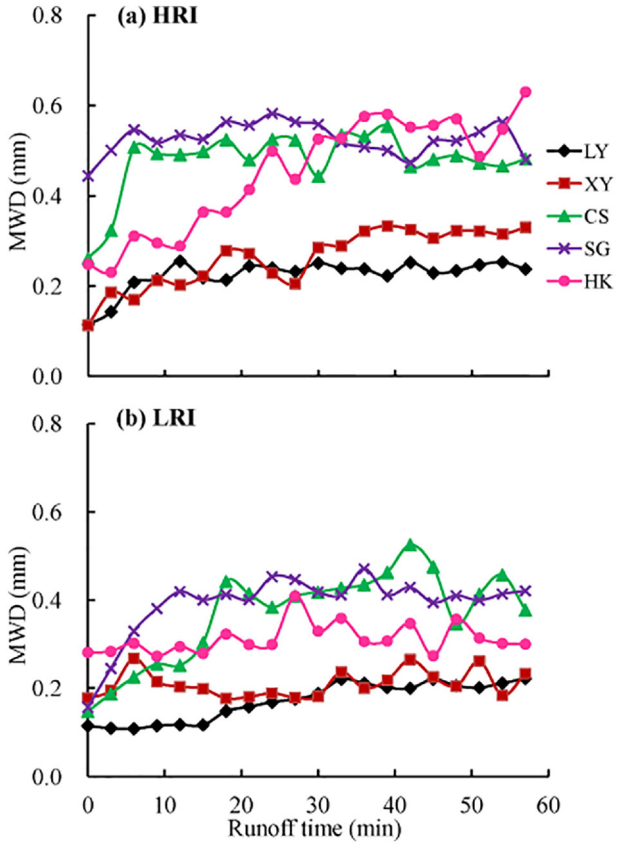

Fig. 9. Temporal variations in mean weight diameter (MWD) of sediments for different soil types and rainfall intensities (n = 2). LY, Calcic Luvisol; XY, Ferric Luvisol; CS, Plinthic Alisol; SG, Plinthic Acrisol; HK, Acric Ferralsol; HRI, high rainfall intensity (90 mm h^{-1}); LRI, low rainfall intensity (45 mm h^{-1}).

and at the low rainfall intensity, but by the larger size sediment (>0.1 mm) at the steady state at the high rainfall intensity. For HK at the steady state the sediments were dominated by the >0.1 mm size and at the high rainfall intensity, the 1–0.5 mm size sediments occupied >20% of the total sediment mass.

The sediment size was bimodally distributed in most cases except at the early stage or at the low rainfall intensity (Fig. 8). These two peaks were located at the <0.10 mm and 1–0.5 mm size fractions, respectively. The proportion of the <0.10 mm size sediments gradually decreased while that of 1–0.5 mm size sediments increased from LY to HK. For example, the percentage of the 1–0.5 mm size sediments varied in 7–11% for LY, but in 19–27% for HK at the steady state under the high rainfall intensity.

As shown in Fig. 9, the average sediment size increased initially and then approached a relatively fluctuating-steady state. At the high rainfall intensity, the mean weight diameter (MWD) of eroded sediments gradually increased from LY to HK at the steady state (Fig. 9-a), but decreased in the order of SG, CS > HK > XY, LY at the low rainfall intensity (Fig. 9-b). The MWD was larger at the high than at the low rainfall intensity (1.2–1.4 times for the average values). The MWD of sediments (0.11–0.58 mm) was much lower than that (0.35–1.78 mm) of water-stable aggregates in the original soils (Table 2) and the difference in MWD between sediments and original soil was least for LY and largest for HK. Relative to sediment yield, the sediment size variation trend of soil types along the climate gradient was more distinct, which is similar to the spatial variation of aggregate water stability. These results showed that sediment size was intrinsically controlled by soil type and influenced by rainfall intensity as well.

4. Discussion

4.1. Effect of soil type and rainfall intensity on runoff

The temporal variation of runoff generation can be explained by the temporal change of surface soil infiltration. The high infiltration capacity under unsaturated surface conditions delayed the runoff generation at the beginning of rainfall. As rainfall continued, soil infiltration was reduced by the formation of soil crusts due to the interaction between soil properties and rainfall characteristics (Carmi and Berliner, 2008; Ran et al., 2012). Relative to rainfall amount, rainfall intensity produced a more remarkable effect on the alteration of surface soil structure according to the time to start runoff (Fig. 3), which is consistent with Wang et al. (2017).

Under pre-wetting treatment at the field moisture content, the breakdown mechanism of surface soil aggregates was mechanical disruption and dispersion by raindrop and flow impact during the rainfall process (Le Bissonnais, 1996; Shi et al., 2010). In this study, aggregate water stability was positively correlated with amorphous iron oxides ($r = 0.98$, $p < 0.01$). In addition, for the pre-wetted soils, the aggregate stability under rainfall was mainly controlled by the soil mechanical strength (Le Bissonnais, 1996) that was negatively related to soil organic matter and swelling clays, and positively to bulk density, non-swelling clay and sesquioxides content (Kemper and Koch, 1966; Sharma et al., 1991; Wu et al., 2016). Soil susceptibility to crust generally decreased with increased aggregate stability and decreased rainfall intensity (Lado and Ben-Hur, 2004; Shi et al., 2010). Surface soils for LY, CS and SG with abundant organic matter and low bulk density were more prone to be compacted and sealed, thus initiating runoff quickly. In contrast, soil aggregates in XY with high bulk density and low organic matter had large resistance to raindrop disruption, leading to delay and reduction of runoff generation. A similar phenomenon was observed for HK rich in sesquioxides and kaolinite, which is consistent with the report by Wakindiki and Ben-Hur (2002) in that the kaolinitic soils had the most stable aggregates. For these soil types, illite content had a positive relationship with runoff coefficient ($p < 0.01$) irrespective of rainfall intensity (Fig. 10). The illite content influenced by soil weathering degree, could reflect the soil properties (such as sesquioxides, base cations) influencing aggregate stability to some extent.

The effect of soil type on runoff was dependent on rainfall intensity. On the one hand, high rainfall intensity contributed to the disruption of more aggregates in the surface soils and facilitated the rapid formation of crust compared to the low rainfall intensity (Lu et al., 2016; Vaezi et al., 2017); on the other hand, the strong erosive force had overridden the difference in aggregate stability among soil types except for HK, resulting in the similar dynamic of runoff coefficients for these soils. In contrast, because of the weak erosive force at the low rainfall intensity, runoff rate was controlled by soil properties (mainly aggregate stability) and varied greatly among soil types (Fig. 4).

4.2. Effect of soil type and rainfall intensity on erosion process

In most cases, sediment concentration increased with runoff coefficient at the early stage of runoff, but decreased with an increased runoff coefficient such as for LY, CS, HK at the high rainfall intensity and XY, SG at the low rainfall intensity, indicating that sediment delivery was a transport-limited regime at the early stage, followed by the shift to a detachment-limited regime (Kinnell, 2005; Assouline and Ben-Hur, 2006). The decline of sediment concentration was attributed to the decrease of erodible materials and surface stabilization due to the sealing (Chaplot and Le Bissonnais, 2003; Lado and Ben-Hur, 2004). In addition, as the rainfall continued, the loose and coarse materials associated with transport by saltation and rolling on the surface provided a degree of protection against soil detachment by raindrop and flow (Kinnell, 2005, 2012). However, the relationship between sediment concentration and runoff coefficient followed an inverse pattern for LY at the low rainfall

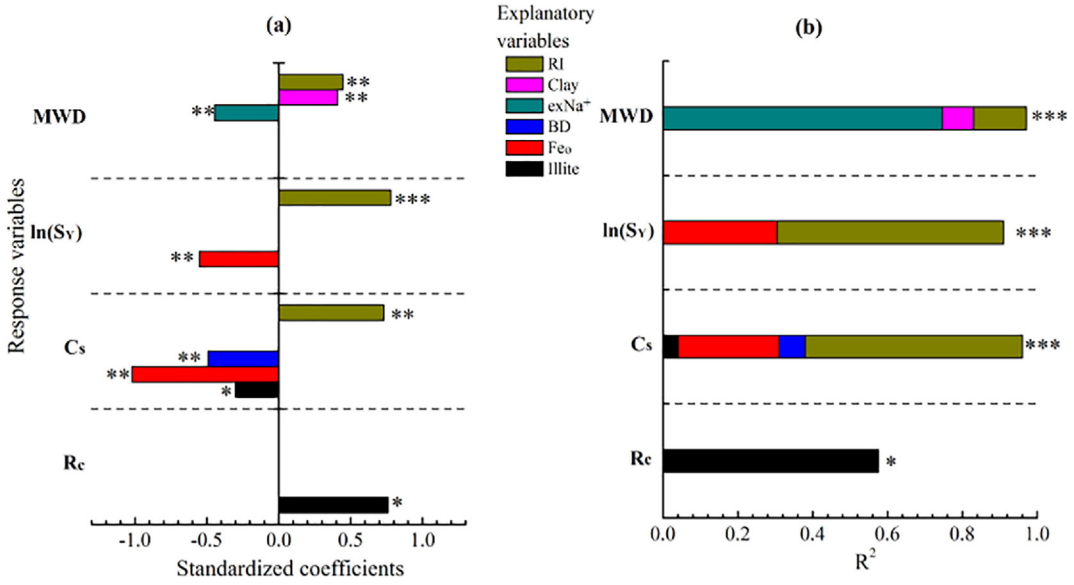

Fig. 10. Multiple stepwise regression results between sheet erosion and soil properties, rainfall intensity (n = 8). (a) Standardized coefficients of variables selected; (b) coefficient of determination (R^2). *, ** and *** indicate the significant level of $p < 0.05$, 0.01 and 0.001, respectively; R_c, the average runoff coefficient; C_s, average sediment concentration; S_Y, average sediment yield rate; MWD, the average mean weight diameter of sediments; RI, rainfall intensity; $exNa^+$, exchangeable sodium; BD, bulk density; Fe_o, amorphous iron oxides; Illite, illite content.

intensity, which could be attributed to the increased transport capacity of surface flow and the sufficient erodible materials in LY.

Sediment concentration was positively correlated with runoff coefficient ($p < 0.01$) for XY at the high rainfall intensity and CS, HK at the low rainfall intensity (Fig. 11-a) (S1 Table), which is consistent with Jin et al. (2008) and Vaezi et al. (2017). In contrast, sediment concentration decreased with an increase of runoff coefficient ($r = -0.76$, $p < 0.001$) for SG at the high rainfall intensity, which could be attributed to the detachment-limited regime due to the crust formation in the rainfall erosion. Soil crusts increased the surface soil shear strength and thus reduced the detachment of surface aggregates in combination with surface loose-coarse materials (Moore and Singer, 1990; Le Bissonnais et al., 2005; Kinnell, 2012). Rainfall intensity played a positive role ($p < 0.001$) while amorphous iron oxides, bulk density and illite content played a negative role in sediment concentration, which accounted for 96% of variance in sediment concentration ($p < 0.001$) (Fig. 10). As the main erosive force, rainfall intensity exerted the dual effects of detaching soil materials and enhancing sediment transport (Zhang and Wang, 2017), which could explain the larger sediment concentration at the high than at the low rainfall intensity. The negative effects of bulk density and amorphous iron oxides were related to their positive roles in soil resistance to erosion through aggregate stability (Sharma et al., 1991; Wu et al., 2016) while high illite content contributed to large overland flow (Fig. 10).

Slightly different from sediment concentration, sediment yield rate was positively correlated with runoff coefficient ($p < 0.05$) except for SG at the high rainfall intensity (Fig. 11-b) (S1 Table), suggesting that raindrop-impact surface flow was the main force in sediment delivery. At the early stage of runoff, the larger sediment yield rate at the high rainfall intensity was mainly attributed to the large transport capacity of surface flow as erodible materials were sufficient. For XY and HK (S1 Table), the correlation coefficient was larger at the high ($r = 0.95$ and 0.94, $p < 0.001$) than at the low rainfall intensity ($r = 0.85$ and 0.86, $p < 0.001$), implying that aggregates were more easily broken down and then transported at the high rainfall intensity (Shi et al., 2012; Zhang and Wang, 2017) while at the low rainfall intensity, the erosive forces such as raindrop impact and surface flow were weak and thus could not detach and transport soil particles for surface aggregates in large stability (Mahmoodabadi and Sajjadi, 2016; Zhang et al., 2017). In contrast, the correlation coefficient was smaller at the high than at the low rainfall intensity for LY, CS and SG, which was ascribed to the difference in the compactness and thickness of crust at different rainfall intensities, implicating that more dense and cohesive crust would be generated at the high than at the low rainfall intensity (Mohamed and Kohl, 1987).

Similar to sediment concentration, rainfall intensity and amorphous iron oxides had the positive and negative effects respectively on sediment yield rate exponentially (Adj-$R^2 = 88\%$, $p < 0.001$) (Fig. 10). As the erosive force, the rainfall intensity ($R^2 = 61\%$, $p < 0.001$) played a more important role in the sediment yield than the amorphous iron oxides ($R^2 = 30\%$, $p < 0.01$), the latter of which reduced sediment yield rate mainly through increasing the aggregate stability. High aggregate stability prevents aggregates from breakdown and crust formation, increases water infiltration and reduces runoff, leading to a decrease in sheet erosion (Le Bissonnais, 1996). The lowest sediment yield in soil HK among the soil types could be attributed to the loose structure and high aggregate stability of the kaolinitic soils rich in sesquioxides (Wakindiki and Ben-Hur, 2002; Ruiz-Vera and Wu, 2006). Collectively, sheet erosion processes were influenced by the interaction of soil properties and rainfall characteristics, with amorphous iron oxides and bulk density enhancing soil resistance to erosive forces along the climatic gradient.

4.3. Effects of soil type and rainfall intensity on sediment size and transport mechanism

The positive correlations between sediment size and runoff coefficient ($p < 0.01$) except for XY and HK at the low rainfall intensity (Fig. 11-c) (S1 Table) indicated that large overland flow facilitated the transport of coarse sediments, which is consistent with Asadi et al. (2007, 2011). Rainfall intensity and clay content exerted a positive role in sediment size while exchangeable Na^+ content had a negative effect (Adj-$R^2 = 0.96$, $p < 0.001$). High rainfall intensity corresponded to the large erosive forces in soil detachment and sediment transport in the rainfall erosion (Zhang and Wang, 2017). The positive effect of clay content on sediment size can be attributed to the large cohesive forces between particles against raindrop and flow destruction (Kemper and Koch, 1966; Meyer and Harmon, 1984). Previous studies reported that the hydration of exchangeable cations and swelling clay minerals weakens the bonds between soil particles (Kemper et al.,

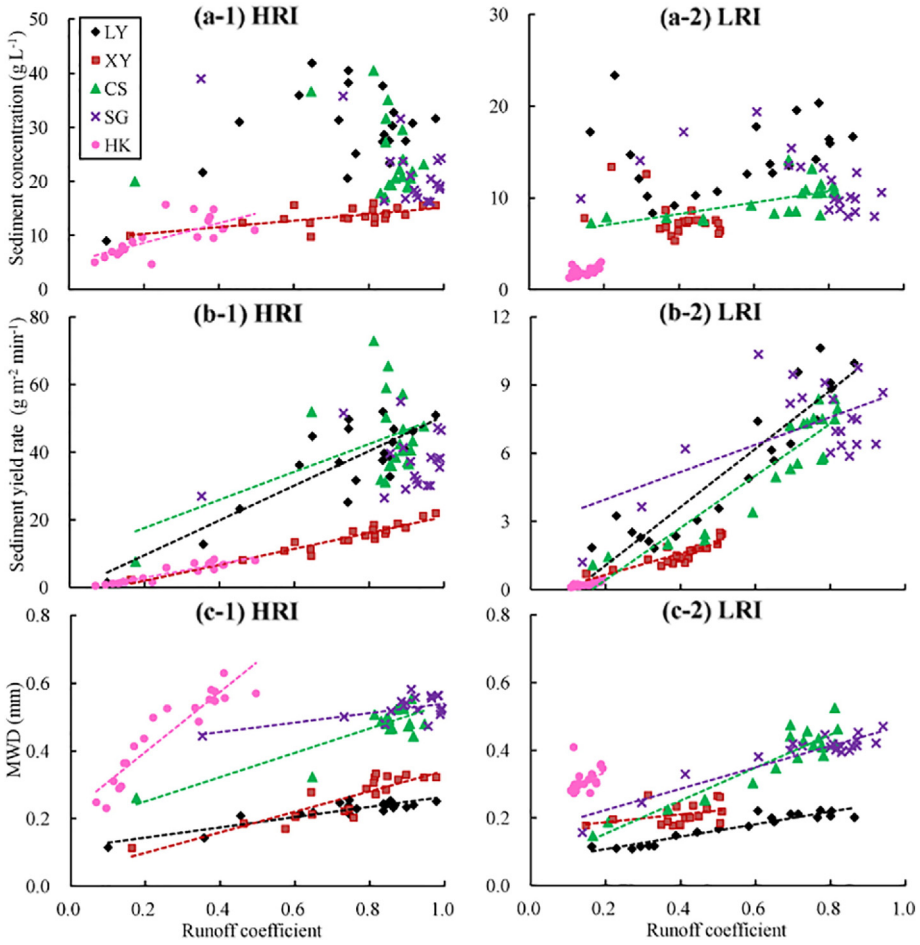

Fig. 11. Relationships between sediment concentration, sediment yield rate, mean weight diameters (MWD) of sediments with runoff coefficient (n = 20). LY, Calcic Luvisol; XY, Ferric Luvisol; CS, Plinthic Alisol; SG, Plinthic Acrisol; HK, Acric Ferralsol; HRI, high rainfall intensity (90 mm h^{-1}); LRI, low rainfall intensity (45 mm h^{-1}).

1987; Mamedov et al., 2002; Reichert et al., 2009). Therefore the large exchangeable Na^+ content along with the swelling clay-vermiculite such as that in LY and XY would contribute to the dispersion of soil particles under the impact of rainfall. As the hydrothermal condition increased from temperate to tropical climate, soil weathering intensity (i.e. desilicification and ferrallitization) increased with sesquioxides accumulating and base cations leaching, which resulted in the increased trend of sediment size from LY to HK.

The bimodal distribution of sediment size in the coarser and finer size fractions results from the transport mechanisms of rolling and suspension/saltation, respectively (Asadi et al., 2007, 2011; Kinnell, 2012; Shi et al., 2012). The bimodal pattern of sediment size distribution generally became more distinct from LY to HK and at the higher rainfall intensity, indicating that sediment transport pattern varied with soil type and rainfall intensity (Wang et al., 2014). Sediment transport was dominated by suspension/saltation for LY and XY and by both mechanisms for the other soils except at the early stage of runoff. The percentage of coarse sediments in rolling increased with the increased flow transport capacity (Kinnell, 2006). According to the temporal variation of sediment size, the relative importance of suspension/saltation (<0.1 mm) decreased with runoff time especially at the early stage of runoff while that of rolling (1–0.5 mm) increased. The difference in the particle travel rates also influences the temporal variation of the sediment size composition (Kinnell, 2006, 2012). Fine particles generally travel in suspension at the velocity of the flow and can be more easily and quickly transported than coarse materials by raindrop-induced saltation and rolling (Kinnell, 2006, 2012). Therefore, the proportion of fine particles was high at the early stage of runoff and that of coarse particles increased as the rainfall continued. Meanwhile, the bimodal distribution of sediment size was also influenced to some extent by the nature of soil hierarchical structure (S1 Fig.) where large aggregates were stepwise disintegrated into smaller aggregates rather than clay or silt particles during the rainfall (Wei et al., 2016).

During the rainfall erosion, the fine sediment fraction (such as <0.1 mm size) would be transported in longer distance due to its lower settling velocity (Asadi et al., 2007; Kinnell, 2012). At the catchment scale, the dominant mechanism for sediment export was suspension of fine particles (<0.1 mm size) in the surface flow (Hancock et al., 2017). These characteristics suggest that more attention should be paid to the off-site impact of soil erosion on LY and XY due to their large fine sediment content and low particle density. Sediment size characteristics under different climate conditions were intrinsically determined by soil properties, especially the exchangeable Na^+ and clay content, and also influenced by rainfall characteristics (intensity and duration).

5. Conclusion

In this study, the effects of soil type and rainfall intensity on sheet erosion processes from the temperate to tropical climate were systematically investigated with the field plot rainfall simulation experiments. High rainfall intensity contributed to runoff generation, sediment concentration and yield. Sediment concentration was the lowest for the Ferralsol and largest for the temperate Luvisol among all soil types. Along with rainfall intensity, clay mineralogy (illite and amorphous iron oxides) and bulk density influenced the hydrological and erosional processes at the soil type scale.

The effective sediment size showed a more distinct upward trend from Luvisol to Ferralsol. The sediment transport was dominated by suspension/saltation (<0.1 mm) for the Luvisols, and by both suspension/saltation (<0.1 mm) and rolling for the other soil types. The sediment size was intrinsically determined by clay content and exchangeable sodium, and enhanced by high rainfall intensity as well. These results will facilitate the understanding of sediment transport behavior from hillslope scale to catchment scale under different climate conditions as well as the effects of past and future climate changes on geo-ecological processes.

Supplementary data to this article can be found online at https://doi.org/10.1016/j.scitotenv.2017.11.202.

Author contributions

Xinliang Wu and Yujie Wei contribute equally to the paper.

Acknowledgements

This work was supported by the National Natural Science Foundation of China (41630858 and 41471231) and the PhD Candidate Research Innovation Project of Huazhong Agricultural University (Program No. 2014bs18). Thanks to Di Wang, Jie Wang, Li She, Yang Zhou, Ya Luo, Zirui Chen and Ze Liu for their assistance in field experiments and laboratory analyses.

References

Asadi, H., Ghadiri, H., Rose, C.W., Yu, B., Hussein, J., 2007. An investigation of flow-driven soil erosion processes at low stream powers. J. Hydrol. 342, 134–142.
Asadi, H., Moussavi, A., Ghadiri, H., Rose, C.W., 2011. Flow-driven soil erosion processes and the size selectivity of sediment. J. Hydrol. 406, 73–81.
Assouline, S., Ben-Hur, M., 2006. Effects of rainfall intensity and slope gradient on the dynamics of the interrill erosion during soil surface sealing. Catena 66, 211–220.
Cai, Q.G., Wang, H., Curtin, D., Zhu, Y., 2005. Evaluation of the EUROSEM model with single event data on steeplands in the Three Gorges Reservoir Areas, China. Catena 59, 19–33.
Carmi, G., Berliner, P., 2008. The effect of soil crust on the generation of runoff on small plots in an arid environment. Catena 74, 37–42.
Cerdà, A., 1998. Relationships between climate and soil hydrological and erosional characteristics along the climatic gradients in Mediterranean limestone areas. Geomorphology 25, 123–134.
Chaplot, V.A.M., Le Bissonnais, Y., 2003. Runoff features for interrill erosion at different rainfall intensities, slope lengths and gradients in an agricultural loessial hillslope. Soil Sci. Soc. Am. J. 67, 844–851.
Defersha, M.B., Melesse, A.M., 2012. Effect of rainfall intensity, slope and antecedent moisture content on sediment concentration and sediment enrichment ratio. Catena 90, 47–52.
Dlamini, P., Orchard, C., Jewitt, G., Lorentz, S., Titshall, L., Chaplot, V., 2011. Controlling factors of sheet erosion under degraded grasslands in the sloping lands of KwaZulu-Natal, South Africa. Agr. Water Manag. 98, 1711–1718.
Ellison, W.D., 1947. Soil erosion studies: I. Agric. Eng. 28, 145–146.
Glendell, M., Brazier, R.E., 2014. Accelerated export of sediment and carbon from a landscape under intensive agriculture. Sci. Total Environ. 476–477, 643–656.
Gumiere, S.J., Le Bissonnais, Y., Raclot, D., 2009. Soil resistance to interrill erosion: model parameterization and sensitivity. Catena 77, 274–284.
Hancock, G.R., Hugo, J., Webb, A.A., Turner, L., 2017. Sediment transport in steep forested catchments-an assessment of scale and disturbance. J. Hydrol. 547, 613–623.
IUSS Working Group WRB, 2014. World Reference Base for Soil Resources 2014. International soil classification system for naming soils and creating legends for soil maps. World Soil Resources Reports No. 106. FAO, Rome.
Jin, K., Cornelis, W.M., Gabriels, D., Shiettecatte, W., Neve, S.D., Lu, J., Buysse, T., Wu, H., Cai, D., Jin, J., Harmann, R., 2008. Soil management effects on runoff and soil loss from field rainfall simulation. Catena 75, 191–199.
Kemper, W.D., Koch, E.J., 1966. Aggregate Stability of Soils From Western USA and Canada. USDA Technical Bulletin No. 1355. US Government Printing Office, Washington, DC.
Kemper, W.D., Rosenau, R.C., 1986. Aggregate stability and size distribution. In: Klute, A. (Ed.), Methods of Soil Analysis: Part 1. Agron. Monogr. 9. ASA and SSA, Madison, WI, pp. 425–442.
Kemper, W.D., Rosenau, R.C., Dexter, A.R., 1987. Cohesion development in disrupted soils as affected by clay and organic matter content and temperature. Soil Sci. Soc. Am. J. 51, 860–867.
Kinnell, P.I.A., 2005. Raindrop impact induced erosion processes and prediction: a review. Hydrol. Process. 19, 2815–2844.
Kinnell, P.I.A., 2006. Simulations demonstrating interaction between coarse and fine sediment loads in rain-impacted flow. Earth Surf. Process. Landf. 31, 355–367.
Kinnell, P.I.A., 2012. Raindrop-induced saltation and enrichment of sediment discharged form sheet and interill erosion areas. Hydrol. Process. 26, 1449–1456.
Kinnell, P.I.A., 2016. A review of the design and operation of runoff and soil loss plots. Catena 145, 257–265.
Kinnell, P.I.A., 2017. A comparison of the abilities of the USLE-M, RUSLE2 and WEPP to model event erosion from bare fallow areas. Sci. Total Environ. 596–597, 32–42.
Knapen, A., Poesen, J., Govers, G., Gyssels, G., Nachtergaele, J., 2007. Resistance of soils to concentrated flow erosion: a review. Earth-Sci. Rev. 80, 75–109.
Lado, M., Ben-Hur, M., 2004. Soil mineralogy effects on seal formation, runoff and soil loss. Appl. Clay Sci. 24, 209–224.
Lal, R., 2001. Soil degradation by erosion. Land Degrad. Dev. 12, 519–539.
Le Bissonnais, Y., 1996. Aggregate stability and assessment of soil crustibility: I. Theory and methodology. Eur. J. Soil Sci. 47, 425–437.
Le Bissonnais, Y., Cerdan, O., Lecomte, V., Benkhadra, H., Souchère, V., Martin, P., 2005. Variability of soil surface characteristics influencing runoff and interrill erosion. Catena 62, 111–124.
Li, X., 1997. Soil Chemistry and Experiment Instruction. China Agriculture Press, Beijing, pp. 229–235 (in Chinese).
Lu, J., Zheng, F., Li, G., Bian, F., An, J., 2016. The effects of raindrop impact and runoff detachment on hillslope soil erosion and soil aggregate loss in the Mollisol region of Northeast China. Soil Tillage Res. 161, 79–85.
Luk, S., Abrahams, A.D., Parsons, A.J., 1986. A simple rainfall simulator and trickle system for hydro-geomorphic experiments. Phys. Geogr. 7, 344–356.
Mahmoodabadi, M., Sajjadi, S.A., 2016. Effects of rain intensity, slope gradient and particle size distribution on the relative contributions of splash and wash loads to rain-induced erosion. Geomorphology 253, 159–167.
Malam Issa, O., Le Bissonnais, Y., Planchon, O., Favis-Mortlock, D., Silvera, N., Wainwright, J., 2006. Soil detachment and transport on field- and laboratory-scale interrill areas: erosion processes and the size-selectivity of eroded sediment. Earth Surf. Process. Landf. 31, 929–939.
Mamedov, A.I., Shainberg, I., Levy, G.J., 2002. Wetting rate and sodicity effects on interrill erosion from semi-arid Israeli soils. Soil Tillage Res. 68, 121–132.
Martínez-Mena, M., Castillo, V., Albaladejo, J., 2002. Relations between interrill erosion processes and sediment particle size distribution in a semiarid Mediterranean area of SE of Spain. Geomorphology 45, 261–275.
Mchunu, C., Chaplot, V., 2012. Land degradation impact on soil carbon losses through water erosion and CO_2 emissions. Geoderma 177–178, 72–79.
Meyer, L.D., Harmon, W.C., 1984. Susceptibility of agricultural soils to interrill erosion. Soil Sci. Soc. Am. J. 48, 1152–1157.
Mohamed, D., Kohl, R.A., 1987. Infiltration response to kinetic energy. Trans. ASAE 30, 108–111.
Moore, D.C., Singer, M.J., 1990. Crust formation effects on soil erosion processes. Soil Sci. Soc. Am. J. 54, 1117–1123.
Nearing, M.A., Pruski, F.F., O'Neal, M.R., 2004. Expected climate change impacts on soil erosion rates: a review. J. Soil Water Conserv. 59 (1), 43–50.
Ran, Q., Su, D., Li, P., He, Z., 2012. Experimental study of the impact of rainfall characteristics on runoff generation and soil erosion. J. Hydrol. 424, 99–111.
Reichert, J.M., Norton, L.D., Favaretto, N., Huang, C., Blume, E., 2009. Settling velocity, aggregate stability, and interrill erodibility of soils varying in clay mineralogy. Soil Sci. Soc. Am. J. 73, 1369–1377.
Rickson, R.J., 2014. Can control of soil erosion mitigate water pollution by sediments? Sci. Total Environ. 468–469, 1187–1197.
Ruiz-Sinoga, J.D., Diaz, A.R., 2010. Soil degradation factors along a Mediterranean pluviometric gradient in Southern Spain. Geomorphology 118, 359–368.
Ruiz-Vera, V.M., Wu, L., 2006. Influence of sodicity, clay mineralogy, prewetting rate, and their interaction on aggregate stability. Soil Sci. Soc. Am. J. 70, 1825–1833.
Salvador Sanchis, M.P., Torri, D., Borselli, L., Poesen, J., 2008. Climate effects on soil erodibility. Earth Surf. Process. Landf. 33, 1082–1097.
Serpa, D., Nunes, J.P., Santos, J., Sampaio, E., Jacinto, R., Veiga, S., Lima, J.C., Moreira, M., Corte-Real, J., Keizer, J.J., Abrantes, N., 2015. Impact of climate and land use changes on hydrological and erosion processes of two contrasting Mediterranean catchments. Sci. Total Environ. 538, 64–77.
Sharma, P.P., Gupta, S.C., Rawls, W.J., 1991. Soil detachment by single raindrops of varying kinetic energy. Soil Sci. Soc. Am. J. 55, 301–307.
Shi, Z.H., Yan, F.L., Li, L., Li, Z.X., Cai, C.F., 2010. Interrill erosion from disturbed and undisturbed samples in relation to topsoil aggregate stability in red soils from subtropical China. Catena 81, 240–248.
Shi, Z.H., Fang, N.F., Wu, F.Z., Wang, L., Yue, B.J., Wu, G.L., 2012. Soil erosion processes and sediment sorting associated with transport mechanisms on steep slopes. J. Hydrol. 454–455, 123–130.
Six, J., Feller, C., Denef, K., Ogle, S., de Moraes Sa, J.C., Albrecht, A., 2002. Soil organic matter, biota and aggregation in temperate and tropical soils-effects of no-tillage. Agronomie 22, 755–775.
Vaezi, A.R., Ahmadi, M., Cerdà, A., 2017. Contribution of raindrop impact to the change of soil physical properties and water erosion under semi-arid rainfalls. Sci. Total Environ. 583, 382–392.
Wakindiki, I.I.C., Ben-Hur, M., 2002. Soil mineralogy and texture effects on crust micromorphology, infiltration, and erosion. Soil Sci. Soc. Am. J. 66, 897–905.
Wang, B., Zheng, F., Römkens, M.J.M., Darboux, F., 2013. Soil erodibility for water erosion: a perspective and Chinese experiences. Geomorphology 187, 1–10.
Wang, L., Shi, Z.H., Wang, J., Fang, N.F., Wu, G.L., Zhang, H.Y., 2014. Rainfall kinetic energy controlling erosion processes and sediment sorting on steep hillslopes: a case study of clay loam soil from the Loess Plateau, China. J. Hydrol. 512, 168–176.
Wang, B., Steiner, J., Zheng, F., Gowda, P., 2017. Impact of rainfall pattern on interrill erosion process. Earth Surf. Process. Landf. https://doi.org/10.1002/esp.4140.

Wei, Y., Wu, X., Xia, J., Shen, X., Cai, C., 2016. Variation of soil aggregation along the weathering gradient: comparison of grain size distribution under different disruptive forces. PLoS One 1–18.
Wu, X., Cai, C., Wang, J., Wei, Y., Wang, S., 2016. Spatial variations of aggregate stability in relation to sesquioxides for zonal soils, South-central China. Soil Tillage Res. 157, 11–22.
Xue, W., 2013. SPSS statistical methods and applications. 3th Edition. Publishing House of Electronics Industry, Beijing, China (in Chinese).
Zhang, G., Gong, Z., 2012. Soil Survey Laboratory Methods. Science Press, Beijing (in Chinese).
Zhang, X.C., Wang, Z.L., 2017. Interrill soil erosion processes on steep slopes. J. Hydrol. 548, 652–664.
Zhang, X.C., Nearing, M.A., Garbrecht, J.D., 2017. Gaining insights into interrill erosion processes using rare earth element tracers. Geoderma 299, 63–72.